UNIVERSITY OF CALIFORNIA
RIVERSIDE

Phosphoproteomic Analysis of the Consequences of Deletion of the Phosphatase, TCPTP, in the Intestinal Epithelium

A Thesis submitted in partial satisfaction
of the requirements for the degree of

Master of Science

in

Biomedical Sciences

by

Akash Lalka

September 2023

Thesis Committee:
Dr. Declan McCole, Chairperson
Dr. Nicholas V. DiPatrizio
Dr. David Lo

The Thesis of Akash Lalka is approved:

Committee Chairperson

University of California, Riverside

Acknowledgements

I would like to thank my mentor, Dr. McCole for giving me the opportunity to conduct research in his lab and supporting me throughout this journey. I appreciate my lab mates for teaching me the lab protocols and new lab techniques. Thank you to Dr. Lo and Dr. DiPatrizio for guiding me through the final stages of my project. I greatly appreciate the UCR School of Medicine for the two scholarships they awarded me during these two years. Last but not least, this would not have been possible without the support of my parents, Naina and Nitin Lalka, and my friends.

ABSTRACT OF THE THESIS

Phosphoproteomic Analysis of the Consequences of Deletion of the Phosphatase, TCPTP, in the Intestinal Epithelium

by

Akash Lalka

Master of Science, Graduate Program in Biomedical Sciences
University of California, Riverside, September 2023
Dr. Declan McCole, Chairperson

Phosphoproteomic analysis is a relatively recently devised method used to quantify a phosphoproteome (total number of phosphorylated proteins in a sample) and identify specific amino acid residues on proteins that are phosphorylated in order to further analyze their role in cellular processes. Our lab studies the role of the gene, protein tyrosine phosphatase non-receptor Type 2 (PTPN2), in the intestinal epithelium. This gene codes for T-Cell Protein Tyrosine Phosphatase (TCPTP). Loss-of-function mutations in the *Ptpn2* gene locus are associated with an increased risk of developing several auto-inflammatory diseases such as Inflammatory Bowel Disease (IBD), Celiac Disease, Rheumatoid Arthritis, and Type 1 Diabetes. Considering that our candidate gene codes for a phosphatase, we can hypothesize that this will have effect on the quantity and identity of phosphopeptides present. We hoped to find out how changes in the phosphoproteome in *Ptpn2* knockout (KO) mice compared to wild type (WT) mice. Surprisingly, we found no significant changes in the quantity of phosphoproteins and their residues, no significant changes in phosphorylation of TCPTP substrates, and no

significant changes in the pathways identified as a result of the phosphorylated proteins between the two groups.

Table of Contents:

List of Figures

INTRODUCTION

The intestinal epithelium is comprised of a tight layer of intestinal epithelial cells (IECs) that selectively uptake nutrients and electrolytes, prevents the entry of pathogens, and regulates immune cell function. This barrier is maintained by tight junctions which restrict the paracellular permeability between IECs. The tight junction is made up of transmembrane proteins including members of the claudin family of proteins, occludin, JAM proteins, and tricellulin. These proteins form complexes with zonula occludin (ZO) molecules to support the function of the tight junction (Spalinger et al., 2020). Disturbance of the tight junction can lead to increased permeability to nutrients, electrolytes, pathogens, and other macromolecules. This can in turn lead to the activation of the mucosal immune system, resulting in inflammation and tissue damage, as well as the development of chronic inflammatory conditions such as inflammatory bowel disease (IBD) (Marchelletta et al., 2021). One of the pathways that is involved in tight junction regulation is the janus kinase and signal transducer and activator of transcription (JAK-STAT) pathway. This pathway is regulated by the gene, protein tyrosine phosphatase non-receptor Type 2 (*Ptpn2*). This gene codes for T-cell protein tyrosine phosphatase non-receptor type 2 (TCPTP), a protein that is a key player in maintaining the homeostasis of the intestinal epithelium. This pathway modulates cytokine signaling and cellular proliferation. TCPTP dephosphorylates JAK and STAT proteins, subduing their functions, and keeping an intact epithelium without excess inflammation. The upregulation of the JAK-STAT pathway driven by the loss of *Ptpn2*, worsens the responses to pro-inflammatory cytokines such as interferon gamma (IFN-γ). IFN-γ also

increases the binding of STAT1 to the Claudin-2 promoter, thereby increasing transcription and subsequent protein expression of this cation pore-forming tight junction protein (Sayoc-Becerra et al., 2020). Functionally, this results in increased paracellular flux of sodium and subsequent exit of chloride and water into the intestinal lumen, leading to diarrhea (Sayoc-Becerra et al., 2020). This increase in claudin-2 mediated epithelial permeability contributes to what is colloquially referred to as "leaky gut", and is a hallmark of IBD (Sayoc-Becerra et al., 2020). *Ptpn2* is also a regulator of immune cell function and can aid in preventing the onset of cancer (Spalinger et al., 2018).

Loss of *Ptpn2* leads to increased tyrosine phosphorylation of its substrates. Therefore, identifying the full suite of phosphorylation changes arising from loss of *Ptpn2* expression or activity is an important goal in order to understand the full complement of biological changes resulting from loss of *Ptpn2*. Phosphoproteomic analysis is becoming an increasingly essential method in studying physiological processes moderated by cellular signaling. It is the study of identification and characterization of phosphorylated peptides and proteins. Protein phosphorylation, characterized by the addition of a phosphate group to a protein by a kinase, is an essential post-translational modification responsible for regulating signaling mechanisms and in turn, physiological processes. They are mostly phosphorylated on Serine, Threonine, and Tyrosine amino acids. Proteins can also be phosphorylated on Histidine, Cysteine, Aspartic acid, and Arginine residues. However, our understanding of how phosphorylation of these residues contributes to biological properties is poorly understood. Proteins can also be dephosphorylated by other proteins called phosphatases,

such as TCPTP (McCole, 2013). Phosphorylation usually activates a protein, whereas dephosphorylation usually inactivates a protein. Nonetheless, both processes can either activate or inactivate a protein. Dysregulation of the phosphorylation of certain proteins have been determined to cause many diseases, including cancer. Thanks to this approach, many kinase inhibitors have been developed to ameliorate such diseases. For a long time, phosphorylation has been studied at a basic, singular protein level. However, mass spectrometry has allowed for large-scale profiling of a multi-cellular proteome (total number of proteins in a sample) and phosphoproteome (total number of phosphorylated proteins in a sample) (Savage and Zhang, 2020). This analysis involves the identification, quantification, and localization of the phosphate group of phosphopeptides. Localization of the phosphosite is especially important because the phosphorylation of different amino acids on a protein can have differing effects on that protein's function. After these initial steps, the data are then interpreted into physiological and clinical insights (Savage and Zhang, 2020). This usually requires the utilization of a secondary software, such as Ingenuity Pathway Analysis (IPA), in order to visualize the kinases that phosphorylated the proteins in a dataset and if that is associated with upregulation or downregulation of a signaling pathway. Even though the TCPTP-JAK-STAT network is an important pathway of focus in our lab, it can be inferred that there are other phosphorylation-mediated pathways yet to be discovered that regulate the homeostasis of the intestinal epithelium. The goal of this study was to identify the broader set of proteins whose phosphorylation is altered by the loss of TCPTP expression. To achieve this, we isolated

intestinal epithelial cells (IECs) from small and large intestine of *Ptpn2*-wild-type (WT) and intestinal epithelial cell specific *Ptpn2*-knockout (KO) mice.

METHODS

Mice

For scraping vs cell recovery solution comparison experiments, Balb/c *Ptpn2* WT and heterozygous (HET) mice were used, respectively. With the cell recovery solution (#354253; Corning; Corning, NY) method, small intestinal (ileum) and large intestinal (cecum and colon) tissue were dissected, washed with PBS, inverted, and placed in cell recovery solution for 2 hours on ice. They were then thoroughly shaken with forceps to release the IECs into the solution. Intestines were removed and the samples were centrifuged at 1.5 x g for 10 minutes at 4°C. IECs were washed twice with ice-cold PBS. Supernatant was removed and RIPA buffer (150 mmol/L NaCl, 5 mmol/L EDTA, 50 mmol/L Tris, 1% NP-40, 0.5% sodium-deoxycholate, and 0.1% sodium dodecyl sulfate) complemented with protease inhibitor cocktail (Roche, Mannheim, Germany); 2 mmol/L sodium fluoride, 1 mmol/L phenylmethylsulfonyl fluoride, 2 mmol/L sodium orthovanadate, and phosphatase inhibitor cocktails 2 and 3 (P5726 and P0044, respectively; Millipore Sigma, Israel) was used to lyse cells (Canale et al., 2023). Cells were immediately frozen. The scraping method was adapted from a previous study (Altay et al., 2020). Tissues were harvested as usual and washed with PBS. Intestinal segments were cut longitudinally and villi were removed by very lightly scraping the mucosa with glass coverslips. Tissues were placed into a petri dish and rinsed with PBS 3 times. Tissue was cut into 1-4mm pieces and added into a conical tube with 10 ml of ice-cold PBS. The tissue solution was vigorously mixed with a pipette to isolate the IECs. Solution was centrifuged, supernatant was removed, and the cell pellet was immediately

frozen. The following day, IECs were homogenized via sonification, centrifuged, and supernatant was collected in new tubes. Protein concentration was assessed with the BCA Protein Assay Kit and loading samples were made by adding loading buffer (60 mM Tris-HCl pH 6.8, 2% SDS, 5% β-mercaptoethanol, 0.01% bromophenol blue, and 10% glycerol) to each sample and boiling them at 95°C for 10 minutes.

For the fibroblast validation, IECs and whole tissue lysates (WTL) were harvested from WT Vil-Cre mice via cell recovery solution method.

For the phosphoproteomic samples, WT and inducible IEC-specific *Ptpn2* KO Vil-Cre mice were used. IECs from the small intestine and large intestine were harvested as above. After the double wash with ice-cold PBS, the cell pellets were immediately frozen. The samples were shipped to UCSD with plenty of dry ice to prevent degradation.

Western Blotting

Loading samples were placed in 7-10% polyacrylamide gels (based on the molecular weight of pertinent proteins) to separate the proteins and were then transferred onto polyvinylidene difluoride membranes. Membranes were blocked with blocking buffer (5% nonfat milk in 1X TBST) for an hour and the incubated with primary antibodies at 4°C overnight according to their corresponding datasheets. The following day, primary antibody solutions were aspirated and membranes were washed with 1X TBST 5 times in 5 minute intervals. Membranes were then diluted in secondary antibody solution for 1 hour followed by another 5 rounds of washing. Membranes were prepared with chemiluminescence solution and exposed to radiographic film to reveal and

visualize the blots. Densitometric analysis was performed for certain experiments using ImageJ software.

Antibodies:

NKCC1 antibody was developed and kindly provided by Dr. Christian Lytle at UCR. The rest of the antibodies used are listed below:

Antibody	**Company**	**Catalog No.**
B-Actin	Sigma; St. Louis, MO	A5316
TCPTP	Cell Signaling Technology; Danvers, MA	58935
STAT1	Cell Signaling Technology	14994
p-STAT1	Cell Signaling Technology	9167
STAT3	Cell Signaling Technology	9139
p-STAT3	Cell Signaling Technology	9145
Vimentin	Cell Signaling Technology	5741
α-SMA	Sigma	A2547
EpCAM	Cell Signaling Technology	42515
ALP1	Invitrogen; Waltham, MA	PA5-2210
Phospho-tyrosine	Cell Signaling Technology	9411

Mass Spectrometry

Mass Spectrometry was performed at the Biomolecular and Proteomics Mass Spectrometry Facility at University of California, San Diego (UCSD). Sample preparations: Samples were lyophilized overnight and reconstituted in 200ul of 6M Guanidine-HCl. The samples were then boiled for 10 minutes followed by 5 minutes cooling at room temperature. The boiling and cooling cycle was repeated a total of 3 cycles. The proteins were precipitated with addition of methanol to a final volume of 90% followed by vortex and centrifugation at maximum speed on a benchtop microfuge (14000 rpm) for 10 minutes. The soluble fraction was removed by flipping the tube onto an absorbent surface and tapping to remove any liquid. The pellet was suspended in 200ul of 8 M Urea made in 100mM Tris pH 8.0. TCEP was added to final concentration of 10 mM and Chloro-acetamide solution was added to final concentration of 40 mM and vortex for 5 minutes. 3 volumes of 50mM Tris pH 8.0 were added to the sample to reduce the final urea concentration to 2 M. Trypsin was in 1:50 ratio of trypsin and incubated at 37C for 12 hours. The solution was then acidified using TFA (0.5% TFA final concentration) and mixed. The sample was desalted using C18-StageTips (Thermo) as described by the manufacturer protocol. The peptide concentration of sample was measured using BCA. 1-10 mg of protein were extracted from each sample, according to peptide concentration. 80 ug of each sample were used in TMT labeling. TMT16 plex (Thermo P/N A44520**)** labelling was carried out as described by the manufacturer. After the labeling completion, the samples were pooled and the peptides were desalted using 100 mg C18-SPR (waters) as described by the manufacturer protocol. The sample was

lyophilized and phospho-peptides were enriched using High-Select Fe-NTA Phosphopeptide Enrichment (A32992 Thermo Scientific). The enriched phosphopeptide fraction was then further fractionated using Pierce™ High pH Reversed-Phase Peptide Fractionation Kit (Pierce™ High pH Reversed-Phase Peptide Fractionation Kit Catalog number: 84868) was used. Fractionation protocol as described by the manufacturer kit. Eight fractions were generated from this step and were analyzed as follows:

LC-MS-MS: 1 ug of each High pH Reversed-Phase enriched phospho-peptides was analyzed by ultra-high-pressure liquid chromatography (UPLC) coupled with tandem mass spectroscopy (LC-MS/MS) using nano-spray ionization. The nano-spray ionization experiments were performed using an Orbitrap fusion Lumos hybrid mass spectrometer (Thermo) interfaced with nano-scale reversed-phase UPLC (Thermo Dionex UltiMate™ 3000 RSLC nano System) using a 25 cm, 75-micron ID glass capillary packed with 1.7-µm C18 (130) BEH^{TM} beads (Waters corporation). Peptides were eluted from the C18 column into the mass spectrometer using a linear gradient (5–80%) of ACN (Acetonitrile) at a flow rate of 375 µl/min for 120 min. The buffers used to create the ACN gradient were Buffer A (98% H_2O, 2% ACN, 0.1% formic acid) and Buffer B (100% ACN, 0.1% formic acid). Mass spectrometer parameters are as follows; an MS1 survey scan using the orbitrap detector mass range (m/z): 400-1500 (using quadrupole isolation), 60000 resolution setting, spray voltage of 2200 V, Ion transfer tube temperature of 290 C, AGC target of 400000, and maximum injection time of 50 ms was followed by data dependent scans (top speed for most intense ions, with charge state set to only include +2-5 ions, and 5 second exclusion time, while selecting ions with minimal intensities of 50000 at in

which the collision event was carried out in the high energy collision cell (HCD Collision Energy of 38%) and the first quadrupole isolation window was set at 0.8 (m/z). The fragment masses were analyzed in the orbitrap detector (mass range (m/z): automatic scan with first scan at m/z= 100. The resolution was set at 30000. AGC Target set to 30000, and maximum injection time: 54 ms. Protein identification and quantification was carried out using Peaks Studio X (Bioinformatics solutions Inc.).

Global Proteome analysis of TMT labelled sample

The flowthrough peptides from the phospho-peptide enrichment step were fractionated using Pierce™ High pH Reversed-Phase Peptide Fractionation Kit (Pierce™ High pH Reversed-Phase Peptide Fractionation Kit Catalog number: 84868). Fractionation protocol as described by the manufacturer kit. LC-MS-MS: 8 collected fractions were each analyzed by ultra-high-pressure liquid chromatography (UPLC) coupled with tandem mass spectroscopy (LC-MS/MS) using nano-spray ionization. The nano-spray ionization experiments were performed using an Orbitrap fusion Lumos hybrid mass spectrometer (Thermo) interfaced with nano-scale reversed-phase UPLC (Thermo Dionex UltiMate™ 3000 RSLC nano System) using a 25 cm, 75-micron ID glass capillary packed with 1.7-µm C18 (130) BEH^{TM} beads (Waters corporation). Peptides were eluted from the C18 column into the mass spectrometer using a linear gradient (5–80%) of ACN (Acetonitrile) at a flow rate of 375 µl/min for 120 min. The buffers used to create the ACN gradient were Buffer A (98% H_2O, 2% ACN, 0.1% formic acid) and Buffer B (100% ACN, 0.1% formic acid). Mass spectrometer parameters are as follows; an MS1 survey scan using the orbitrap detector mass range (m/z): 400-

1500 (using quadrupole isolation), 60000 resolution setting, spray voltage of 2200 V, Ion transfer tube temperature of 290 C, AGC target of 400000, and maximum injection time of 50 ms was followed by data dependent scans top speed for most intense ions, with charge state set to only include +2-5 ions, and 5 second exclusion time, while selecting ions with minimal intensities of 50000 at in which the collision event was carried out in the high energy collision cell (HCD Collision Energy of 38%) and the first quadrupole isolation window was set at 0.8 (m/z). The fragment masses were analyzed in the orbitrap detector mass range (m/z): automatic scan with first scan at m/z= 100. The resolution was set at 30000. AGC Target set to 30000, and maximum injection time: 54 ms. Protein identification and quantification was carried out using Peaks Studio X (Bioinformatics solutions Inc.).

Experiment Tags:

Sample	TMT tag
F719 (+) IEC SI	TMTpro-126
F720 (-) IEC SI	TMTpro-127N
F721 (+) IEC SI	TMTpro-127C
M722 (-) IEC SI	TMTpro-128N
F723 (-) IEC SI	TMTpro-128C
M724 (-) IEC SI	TMTpro-129N
M725 (+) IEC SI	TMTpro-129C
F719 (+) IEC LI	TMTpro-130N
F720 (-) IEC LI	TMTpro-130C
F721 (+) IEC LI	TMTpro-131N
M722 (-) IEC LI	TMTpro-131C
F723 (-) IEC LI	TMTpro-132N
M724 (-) IEC LI	TMTpro-132C
M725 (+) IEC LI	TMTpro-133N

Raw Proteomic and Phosphoproteomic Data Analysis

False Discovery Rate (FDR) threshold was set at 5%. Protein identification and quantification data from PeaksX Studio software (Bioinformatics Solutions Inc.) were imported into R (v4.2.2) (R Core Team 2022) with the tidyverse package (Wickham et al. 2019). Bar plots were generated using the ggpubr package (Kassambara 2023). The above steps were done by Dr. Brandon Le of the Integrative Genome Biology Bioinformatics Core at UCR. Raw data from PeaksX Studio pertaining to the proteomic and phosphoproteomic analysis were exported into excel documents. Relative abundance of proteins and phosphopeptides were assessed by plotting their mean intensities. The intensity correlates to the “area under the curve”, which translates to the relative abundance. Phospho-ratios were re-calculated using a WT sample as a control before

being entered into the Ingenuity Pathway Analysis (IPA) software for Upstream Regulator and Pathway Analysis. Z-scores in IPA are a statistical measure of how closely the actual expression of phosphopeptides in the dataset determines the upregulation or downregulation of a pathway or upstream regulator based on scientific literature. The methodology for z-score calculation has been detailed previously (Krämer et al., 2014).

Mass Spectrometry for Kinome Study

Samples were processed via Liquid Chromatography-Multiple Reaction Monitoring-Mass Spectrometry (LC-MRM-MS). Raw, unnormalized KD/control ratios were analyzed by Skyline software (MacCoss Lab Software; Seattle, WA).

Statistical Analysis

Statistical comparisons were performed using GraphPad Prism (v10; Dotmatics; Boston, MA) using either Mann-Whitney non-parametric t-tests or Multiple Comparisons Two-Way Anova tests. $P \geq 0.05$ was considered not significant (*$P \leq 0.05$, **$P \leq 0.01$, and ***$P \leq 0.001$).

Study Approval

Mouse experimental protocols were approved by the UCR Institutional Animal Care and Use Committee (IACUC). Animal approval protocol number: A20220026.

RESULTS

Purity of isolated intestinal epithelial cell samples

Prior to sending samples for phosphoproteomic analysis, we first confirmed the abundance and purity of IECs isolated from mouse intestines. In addition, we wanted to confirm the presence of phosphorylated proteins in our samples known to be altered by loss of TCPTP expression in order to validate confirmed targets and thereby ensure the highest likelihood of a successful outcome from the phosphoproteomic studies. We compared two different methods for isolating IECs, scraping surface cells from the intestinal mucosa versus our usual method of harvesting IECs via cell recovery solution (Altay et al., 2020).

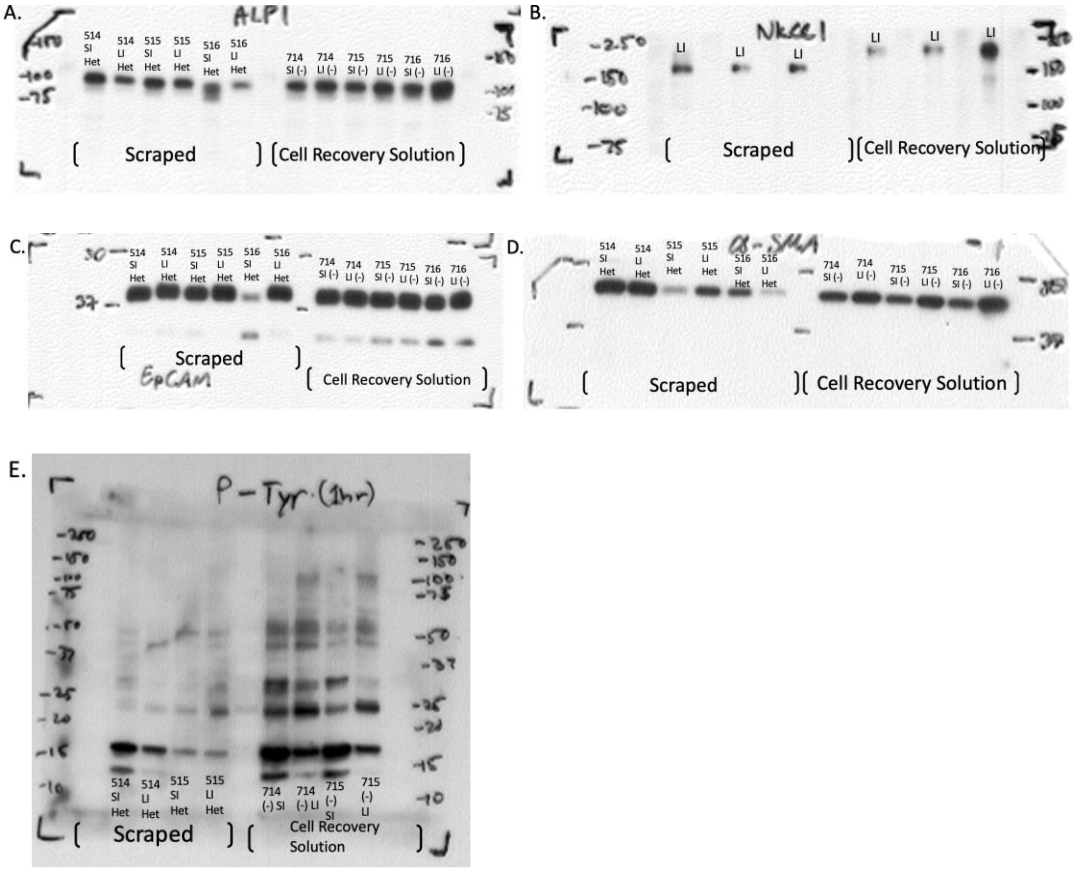

Figure 1: Western Blots of IEC Markers compared between Scraping and Cell Recovery Solution methods:
Blot A shows the difference of ALP1 (marker of Villi-based cells) abundance between IECs from scraping vs cell recovery solution. Blots B, C, D, and E show the difference in abundance of NKCC1 (marker of crypt-based cells), EpCAM (marker for epithelial cells), alpha-sma (marker for mesenchymal cells), and phospho-tyrosine (marker for proteins that exhibit tyrosine phosphorylation) respectively, between both methods. SI indicates small intestine and LI indicates large intestine. (-) indicates a wild type mice and Het indicates a heterozygous mice. Molecular weights of the protein markers are indicated on the left and right sides of the blots. Samples are from Balb/c *Ptpn2* WT and Het mice.

The ALP1, NKCC1, EpCAM, and alpha-sma blots did not show much difference between either method. However, cells from the cell recovery solution method clearly showed more tyrosine phosphorylation. This indicated that cells isolated using recovery solution were more suited for phosphoproteomic analysis. Despite this, the high

abundance of alpha-sma in our cells was concerning because we did not want significant contamination of other cell types, specifically fibroblasts, for which alpha-sma is a marker. This prompted us to further assess the purity of IECs in our samples. CD90 was a common fibroblast marker but after doing further research, Vimentin turned out to be a more reliable marker (Ostrowska-Podhorodecka et al., 2022).

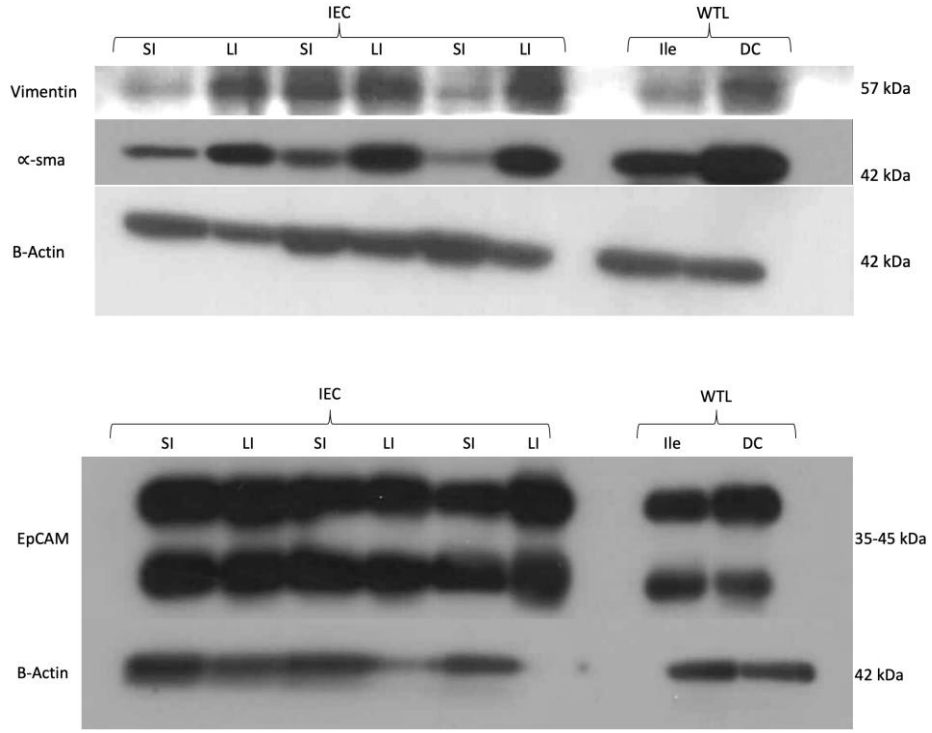

Figure 2: Vimentin Fibroblast Validation
The first set of blots show Vimentin (fibroblast) abundance, alpha-sma (mesenchymal cell) abundance, and Beta-Actin (control) abundance in IECs from the SI and LI (large intestine) and WTLs (whole tissue lysates) from the Ile (Ileum) and DC (Distal Colon). Second set shows EpCAM (epithelial cell) abundance. IECs here were harvested via cell recovery solution. Molecular weights of the protein markers are listed on the right side of the blots. Samples are from WT Vil-Cre mice.

As shown in Figure 2, there was some fibroblast contamination in our IECs. However, there is an overwhelming abundance of epithelial cells as well. We deemed this to be satisfactory for analysis. With this in mind, we decided to submit Vil-Cre WT and

Ptpn2 KO (*Ptpn2* only knocked out in IECs) small and large intestinal samples for mass-spectrometry proteomic and phosphoproteomic analysis. Proteomic analysis was done so we could determine whether the amount of phosphorylation was affected by the relative abundance of the actual protein.

Quantification of TCPTP-regulated Proteome and Phosphoproteome Profiles of Epithelial Cells in Different Intestinal Regions

The first step after receiving the raw data from UCSD was to determine the amount of proteins/peptides and phosphoproteins/phosphopeptides to see if there were any global differences between WT and KO samples. In addition to proteomic and phosphproteomic differences determined by genotype, we also examined if differences occurred between different intestinal segments by comparing data between small intestine (SI) and large intestine (LI). Sex as a variable was also factored into the analysis.

A. Phosphoproteomic Quantification

TMTTag	protein_count	peptide_count	Sample
TMT16-126	2778	15663	F719 (+) IEC SI
TMT16-127C	2804	15879	F721 (+) IEC SI
TMT16-127N	2801	15850	F720 (-) IEC SI
TMT16-128C	2804	15908	F723 (-) IEC SI
TMT16-128N	2799	15833	M722 (-) IEC SI
TMT16-129C	2809	15910	M725 (+) IEC SI
TMT16-129N	2801	15839	M724 (-) IEC SI
TMT16-130C	2801	15901	F720 (-) IEC LI
TMT16-130N	2801	15877	F719 (+) IEC LI
TMT16-131C	2802	15900	M722 (-) IEC LI
TMT16-131N	2802	15885	F721 (+) IEC LI
TMT16-132C	2796	15860	M724 (-) IEC LI
TMT16-132N	2801	15862	F723 (-) IEC LI
TMT16-133N	2802	15903	M725 (+) IEC LI

B. Proteomic Quantification

TMTTag	protein_count	peptide_count	Sample
TMT16-126	5476	39948	F719 (+) IEC SI
TMT16-127C	5503	40268	F721 (+) IEC SI
TMT16-127N	5500	40223	F720 (-) IEC SI
TMT16-128C	5507	40311	F723 (-) IEC SI
TMT16-128N	5505	40244	M722 (-) IEC SI
TMT16-129C	5503	40290	M725 (+) IEC SI
TMT16-129N	5501	40220	M724 (-) IEC SI
TMT16-130C	5505	40293	F720 (-) IEC LI
TMT16-130N	5502	40302	F719 (+) IEC LI
TMT16-131C	5503	40292	M722 (-) IEC LI
TMT16-131N	5503	40297	F721 (+) IEC LI
TMT16-132C	5504	40277	M724 (-) IEC LI
TMT16-132N	5499	40252	F723 (-) IEC LI
TMT16-133N	5505	40293	M725 (+) IEC LI

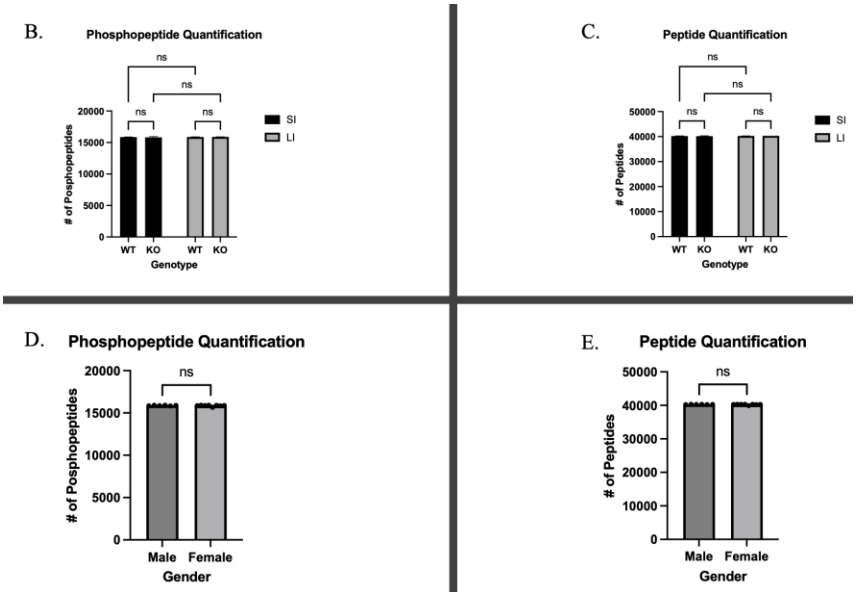

Figure 3: Quantification of Proteome and Phosphoproteome

Table A shows the total number of phosphoproteins and phosphopeptides and Table B shows the total number of proteins and peptides. Samples listed in rightmost columns. "M" signifies a male mouse and "F" signifies a female mouse. (-) denotes a WT sample and (+) denotes a KO sample. Graphs B-E shows statistical comparisons between Genotype, intestinal segments, and sex in peptides and phosphopeptides.

A.

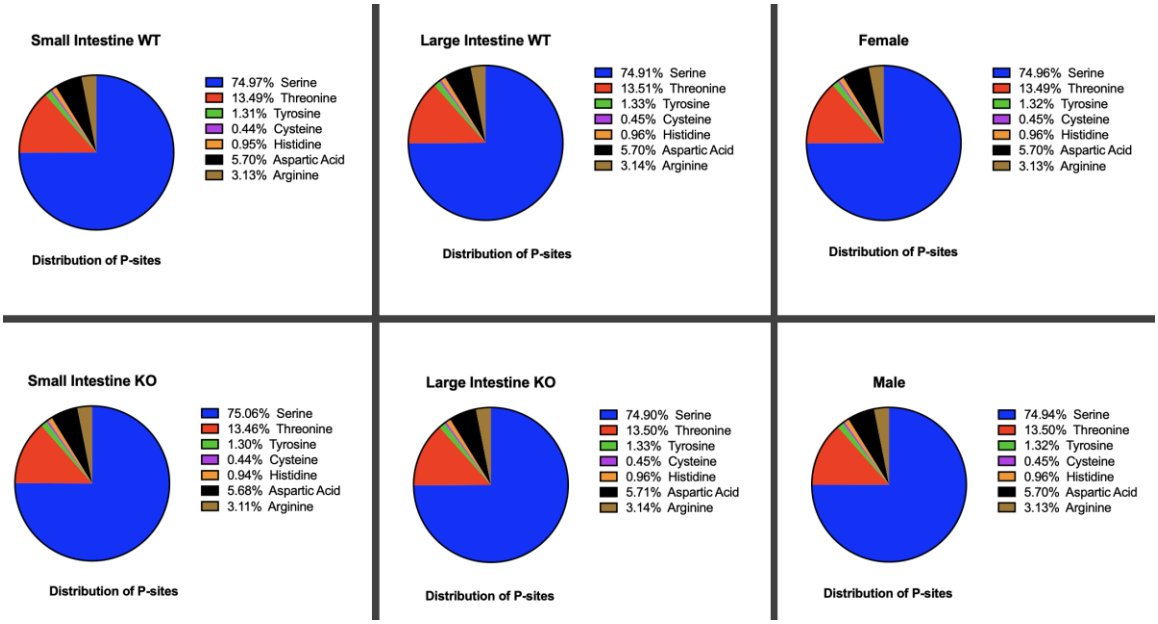

B.

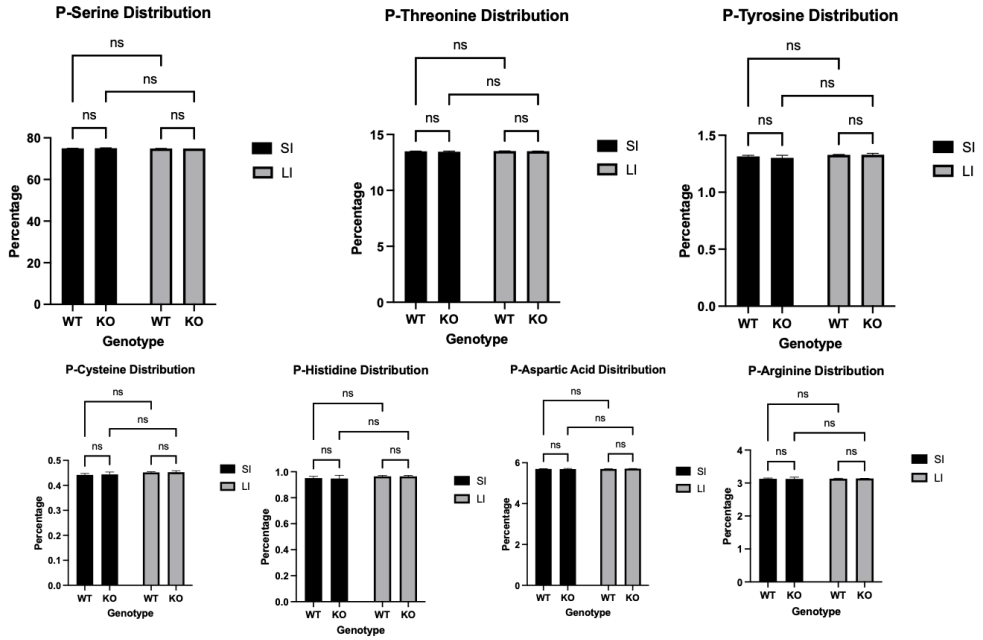

Figure 4: Distribution of the different phosphorylated amino acids
Image A shows pie charts of the distribution of phosphorylated amino acid by percentage between genotype, intestinal segment, and gender. Image B shows the corresponding statistical comparisons.

Evidently, there were no significant changes in the quantification of the proteome and phosphoproteome between genotype, intestinal segment, and gender. We hypothesized that there would be significantly more P-Tyrosine residues in KO samples since TCPTP, a tyrosine phosphatase, is knocked out. Surprisingly however, no overall difference in the abundance of phosphorylated tyrosine resides was observed between WT and KO mouse intestinal samples. Non-canonical phosphorylation of Histidine, Cysteine, Aspartic Acid, and Arginine (HCDR) residues has been mostly studied in prokaryotes but it is evident in eukaryotes (some evidence in human cells) as well. One study showed that histidine phosphorylation on kinases themselves regulated protein structure and dynamics (Hardman et al., 2019). Another study demonstrated that cysteine phosphorylation played a role in cellular signaling and responses (Buchowiecka 2014). Histidine and aspartic acid phosphorylation were shown to regulate cellular shape and motility in human prostate cancer cells (Lapek Jr. et al., 2015). Lastly, multiple arginine phosphorylations of Histone 3 alters its DNA binding ability and chromatin structure (Fuhrmann et al., 2015). Research on HCDR phosphorylation may be gaining popularity, but these residues were not further considered for the purposes of this study. Proteins are known to be differentially phosphorylated based on their localization, function, etc. With the Mass Spec. setup that our samples were processed by, we were unable to see differentially phosphorylated proteins due to trypsin digestion. Trypsin digestion is the process by which proteins are cleaved at lysine and arginine residues and fragmented into peptides. The peptides are then enriched and processed via mass spec. (Gilmore et al.,

2012). Because of this process, we were only able to see differentially phosphorylated peptides.

Absence of altered tyrosine phosphorylation of established TCPTP substrates

We treated STAT1 and STAT3 as positive controls in our analysis since they are well established substrates that are dephosphorylated by TCPTP. Our lab has previously shown that STAT1 and STAT3 exhibit increased phosphorylated Tyr701 and Tyr705, respectively, when *Ptpn2* is knocked out ((Krishnan & McCole, 2017); Canale et al., 2023). The raw phosphopeptide data revealed that these residues were not phosphorylated. Consequently, I used protein samples from the same mice that were used to harvest tissue for the Mass Spec. to probe for these phosphorylated residues.

A.

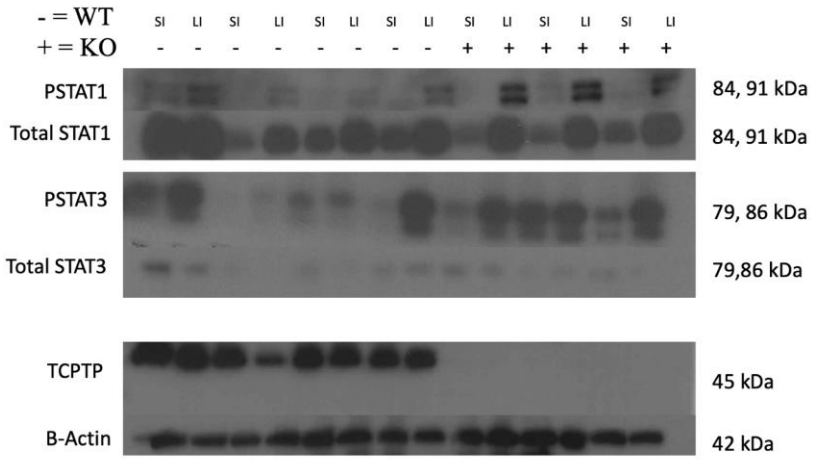

B.

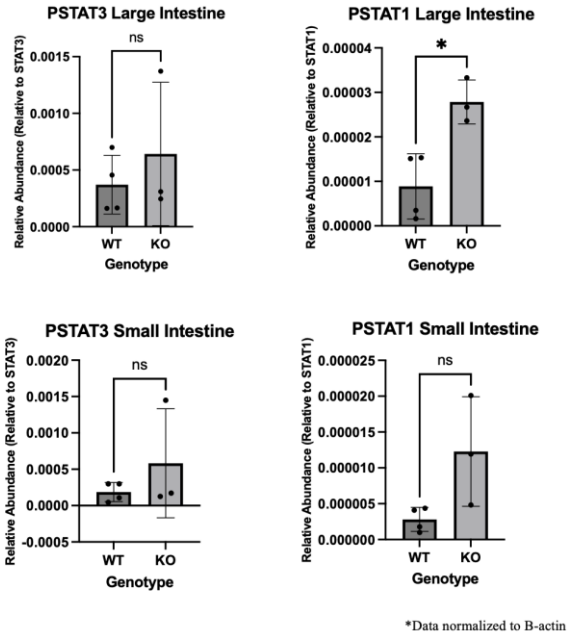

Figure 5: Western Blot and Densitometric Analysis of phosphorylated STAT1 (p-STAT1) and phosphorylated STAT3 (p-STAT3).
Image A shows blots for p-STAT1/STAT1, p-STAT3/STAT3, TCPTP, and B-actin for control. The – symbol indicates a WT sample and the + indicates a KO sample. Image B shows densitometric analysis for the blots.

As shown in Image A and B (Figure 5), there is an increase in p-STAT1 and p-STAT3 in KO samples, with p-STAT1 in the LI being significantly more abundant in KO samples compared to WT. The fact that the STAT1/STAT3 P-tyr peptides did not show up in the Mass Spec. data was concerning, especially because they are fundamental and well-verified focal points of our lab's research. The JAK-STAT pathway plays a very prominent role in homeostatic and inflammatory responses of the intestinal epithelium. Therefore, this raised significant concerns regarding false negative data generated by the phosphoproteomic analysis and suggested that other phosphorylated peptides were similarly not detected and other potentially important pathways may not have been identified. With this major caveat in mind, we proceeded to further analyze the existing phosphoproteomic dataset to identify if any physiological pathways were altered based on *Ptpn2* loss and any associated upstream kinases.

TCPTP substrates showed some significant differences between genotypes

Expanding on the STAT1 and STAT3 analysis above, we looked at their phosphorylated peptides and we also looked at JAK1 and JAK2. JAK3, another established substrate of TCPTP, was not identified in the dataset.

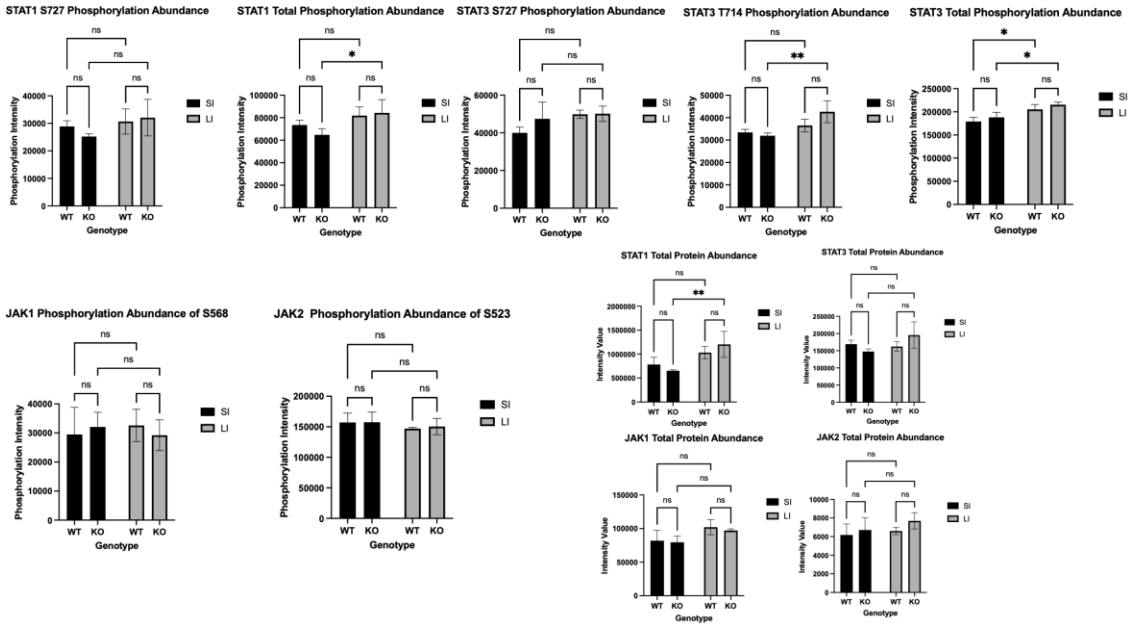

Figure 6: TCPTP deletion seldom affected Ser/Thr phosphopeptides, phosphoproteins, or total protein abundance of STAT1, STAT3, JAK1, and JAK2. Each abundance graph was made by taking the mean of peptide intensity values. "S" indicates a Serine residue and "T" indicates a Threonine residue. Statistical comparisons were made between WT and KO in both intestinal segments and between wild types and knockouts across each segment.

STAT1: STAT1 was significantly more phosphorylated in KO LI samples compared to KO SI samples, but this may be due to the higher total protein abundance between the two conditions (Figure 6). STAT1 phosphorylation at the Serine 727 (S727) position was notable. The phosphorylation of this site by the p38 MAPK kinase has been shown to occur in response to IFN-γ and promote macrophage activation and further inflammatory responses (Kovarik et al., 1999). Phosphorylation at this site by CDK8 has also been shown to elevate cellular proliferation, especially in acute myeloid leukemia cells (Nitulescu et al., 2017). The phosphorylation of this site was not altered in spite of the importance of these pathways.

STAT3: Phosphorylation of S727 on STAT3 has also been shown to activate STAT3. Dysregulation of this phosphosite has been implicated in cancers arising from hampered Epithelial–mesenchymal transition (EMT)/mesenchymal–epithelial transition (MET) processes (Lin et al., 2021).Phosphorylation of S727 has also been observed to cause the translocation of STAT3 to the mitochondria and mediate optimal electron transport chain function (Kim et al., 2018). Nonetheless, the abundance of this phosphosite was constant. Phosphorylation abundance of Threonine-714 (T714) on STAT3 was significantly higher in the LI KO condition compared to SI KO, however, the functional importance of this site has not been well studied. Even though total STAT3 abundance was unchanged in all samples, total phosphorylation of STAT3 was elevated in the large intestine in both genotypes according to the mass spec. data (Figure 6), indicating that STAT3 phosphorylation may be of greater functional importance in the large intestine.

JAK1 & JAK2: The only two phosphosites identified on JAK1 and JAK2 were S568 and S523, respectively. We expected to see increased tyrosine phosphorylation on JAK1, but those residues were not present in the mass spec. data. Phosphorylation of S568 on JAK1 has not been well studied and was unaltered. Phosphorylation of S523 on JAK2 is catalyzed by extracellular signal-regulated kinases or MAPK kinases, and has been shown to inhibit its activity in response to growth hormone (Mazurkiewicz-Munoz et al., 2006). P-S523 was also unchanged, though. There were no total protein differences for JAK1 and JAK2 as well. Here, we showed that other upregulated phospho-sites on TCPTP substrates have functional importance.

Mass spec. analysis identified differences in tight junction protein abundance based on intestinal region but not TCPTP expression

As explained above, tight junctions serve an integral role in maintaining the stability of the intestinal epithelium. Subsequently, we investigated the tight junction proteins that were identified by mass spec. analysis.

A.

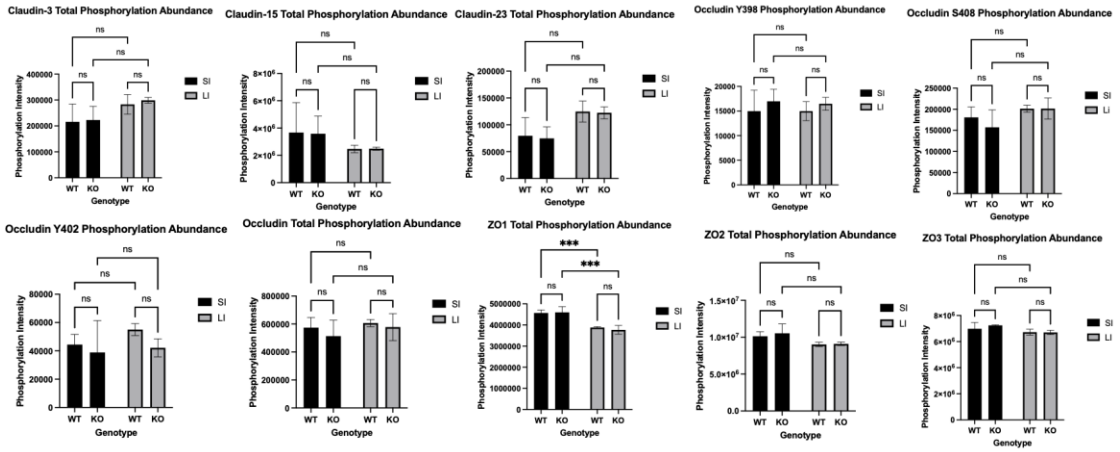

B.

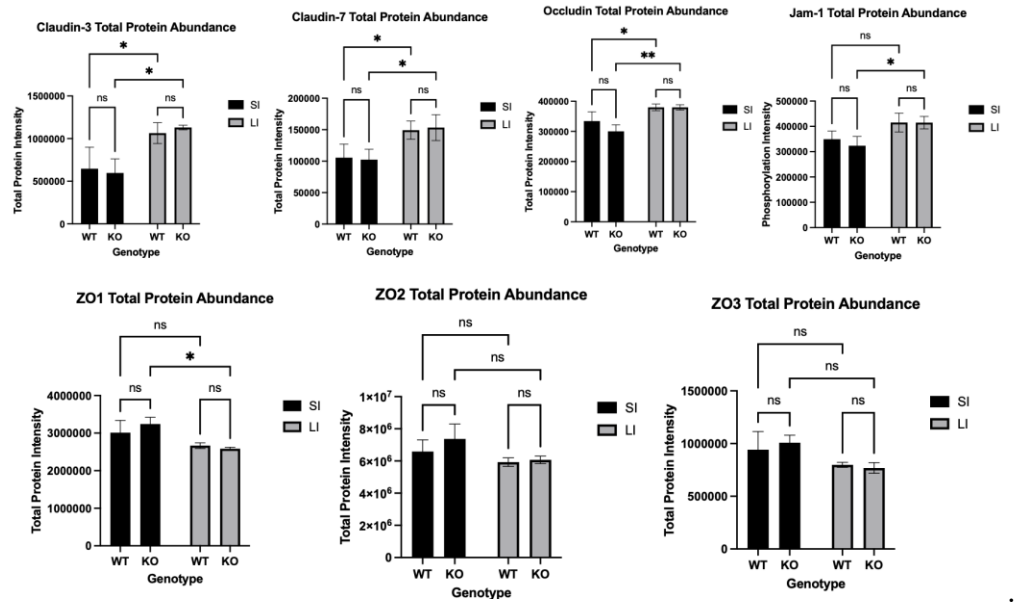

Figure 7: Abundance of tight junction phosphopeptides, phosphoproteins, and total proteins.
Image A portrays phosphorylation abundance of total proteins and specific peptides. Image B portrays the abundance of total proteins. "Y" indicates a tyrosine residue. Statistical comparisons were done as mentioned above.

Claudin-3, Claudin-15, and Claudin-23 had hundreds of differentially phosphorylated sites at S, T, and Y residues. Their phosphorylation at such sites affects

their localization and interaction with ZO proteins, regulating barrier function (Shigetomi et al., 2018). Their amount of phosphorylation was unchanged across intestinal segments and genotype. Puzzlingly, Claudin-15 and Claudin-23 were not found in the proteomic analysis, while Claudin-7, an abundant intestinal epithelial claudin, was identified. Claudin-3 and Claudin-7 were both significantly more abundant in the large intestine in both WT and KO samples. The greater abundance of total Claudin-3 in the large intestine did not appear to have much of an effect on the phosphorylation level of Claudin-3, however. ZO-1, 2 and 3 were found to be heavily phosphorylated at hundreds of S, T, and Y sites as well. Interestingly, ZO-1 phosphorylation was extremely more elevated in the small intestine compared to the large intestine in both WT and KO samples (Image A). The increased phosphorylation in SI KO samples may be attributable to the increase in overall protein in the small intestine (especially between the KO samples), but this is not the case for the large intestine. This indicated that phosphorylation of ZO-1 in the small intestine may be of greater functional importance. There were no changes in ZO-2 and 3 phosphorylation levels and total protein levels. Phosphorylation of these scaffolding proteins affect their localization and interaction with cytoskeletal proteins. Phosphorylation of JAM-1, although not found to be phosphorylated in our analysis, is also an important mechanism involved in tight junction integrity (Van Itallie et al., 2017). Total JAM-1 was significantly more elevated in the large intestine compared to the small intestine in KO samples, however. Occludin S408 phosphorylation was consistent across all samples. S408 phosphorylation is functionally important because it disrupts the selective permeability of the intestinal epithelium by promoting paracellular cation flux

via the dissociation of the occludin/ZO-1/claudin-2 complex (Díaz-Coránguez et al., 2019). Phosphorylation of Y398 and Y402 was also unchanged. These sites are functionally important as their modification causes the translocation of occludin from the cytoplasm to the plasma membrane and binding to ZO-1 (Elias et al., 2009). Many threonine phosphosites were also identified, additionally contributing to tight junction stabilization via ZO interaction (Diaz-Coranguez et al., 2019). Overall occludin levels were significantly higher in the large intestine in WT and KO samples, but there were no changes in its phosphorylation levels. In summary, phosphorylation of these tight junction proteins enables their interactions with each other and is essential in regulating the stability of the tight junction. However, the mass spec analysis did not seem sensitive enough to detect any differences in phosphorylation of these proteins between genotypes or intestinal regions apart from ZO-1.

IPA revealed inconclusive and inconsistent pathway and upstream kinase data

As mentioned above, we used IPA to analyze the entire phosphoproteomic dataset to determine the top up/downregulated pathways and upstream kinases.

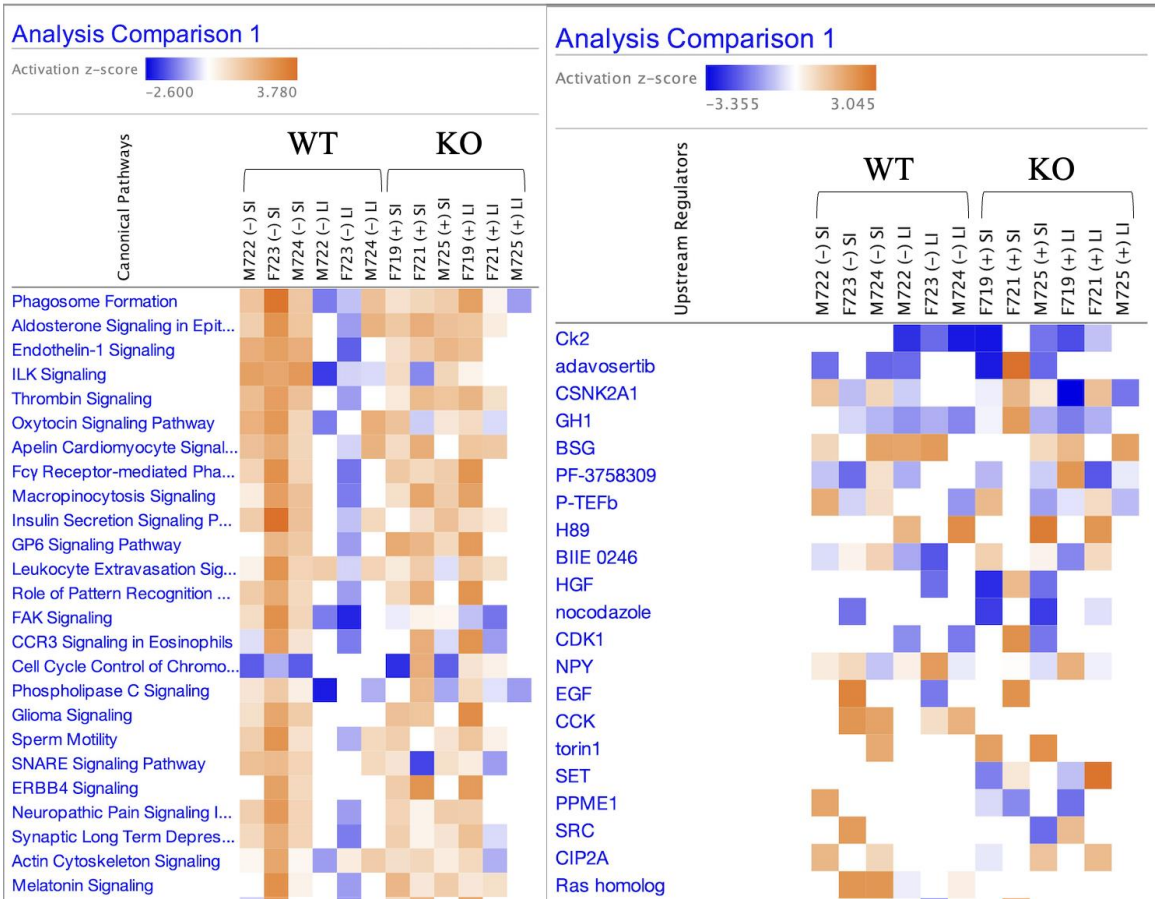

Figure 8: Top identified pathways and upstream regulators
Image on the left shows the top identified pathways and image on the right shows top identified upstream regulators. Colored boxes represent z-scores. A z-score is a statistical measure that represents the significance of the upregulation or downregulation of a pathway or upstream regulator, calculated by IPA. Orange=upregulated and blue=downregulated.

As shown in Figure 8, the data are very inconsistent. Z-scores could not be calculated for some samples, probably due to insignificance with the phospho-ratios for the proteins that are involved in a particular pathway or that are a target of an upstream regulator. In addition, in the left image, the M722 and F723 columns are unexpectedly downregulated. When harvesting tissue from these mice, we noticed that there were two

large, white polyps and a lot of fatty tissue in the intestine. This was abnormal and likely served as macroscopic indicators of more profound physiological and metabolic changes in these mice. We decided to proceed by examining the top four significant upstream regulators and identifying significant pathways pertinent to our lab's studies. Fold changes were calculated from the z-scores to compare the data from WT to KO.

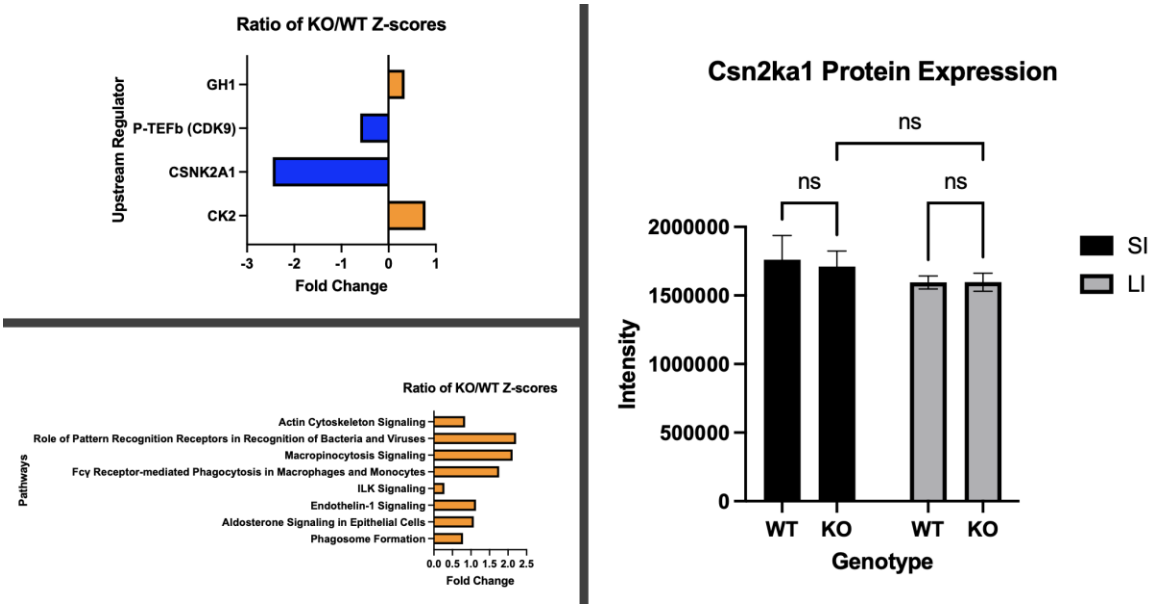

Figure 9: Fold changes of the top upstream regulators and pathways and bar graph abundance of Csn2ka1
Left images show fold changes of the ratio between KO:WT samples for upstream regulators and pathways. Top upstream regulators and pathways were taken from the lists shown in Figure 8. Intestinal segments were not considered because some samples did not have z-scores and we wanted to keep the sample size as high as possible. The bar graph on the right portrays abundance of Csn2ka1 taken from the raw dataset.

Z-scores were used to calculate the ratio between KO/WT for the top upstream regulators and top pathways. It is important to note that the ratios do not reflect the actual expression of the upstream regulators. This was done to more easily visualize changes between KO and WT conditions. The ratio depicts the prediction of whether a certain pathway or upstream regulator was upregulated or downregulated in KO samples

compared to WT samples. Casein Kinase 2 (CK2) was the top "hit". CK2 substrates account for about 20% of the phosphoproteome (Nunez de Villavicencio-Diaz et al., 2015). CK2 did not have much of a change, but its catalytic subunit, Csn2ka1, showed a very steep downregulation (Núñez de Villavicencio-Díaz et al., 2015). While CK2 was just slightly upregulated, Csn2ka1 was markedly downregulated. This may indicate that CK2 is ubiquitously expressed but its catalytic subunit was not very active in KO samples. A closer look into the most significant pathways in the IPA software showed that there were no direct correlations between CK2 and the most upregulated pathways identified by IPA. There seemed to be some disconnection between the top kinases and top pathways. To add to the inconsistencies, total protein abundance (from raw dataset) of Csn2ka1 was relatively constant in WT samples compared to KO samples (Figure 9). CDK9 did not exhibit a marked difference between genotypes so we excluded it as well. Even though growth hormone 1 (GH1) is not a kinase, we initially included it because it is a regulator in the JAK-STAT pathway. For example, GH1 binding to the GH receptor causes phosphorylation of S523 on JAK2, promoting cellular proliferation, differentiation, and survival. However, TCPTP does not dephosphorylate JAK2 (Mazurkiewicz-Munoz et al., 2006). Thus, we excluded it from further analysis as it was not relevant to our studies. Inconsistent data from IPA made it difficult to make distinctions between the genotypes and intestinal segments of our samples. Next, we analyzed some the top targets of Csn2ka1.

A.

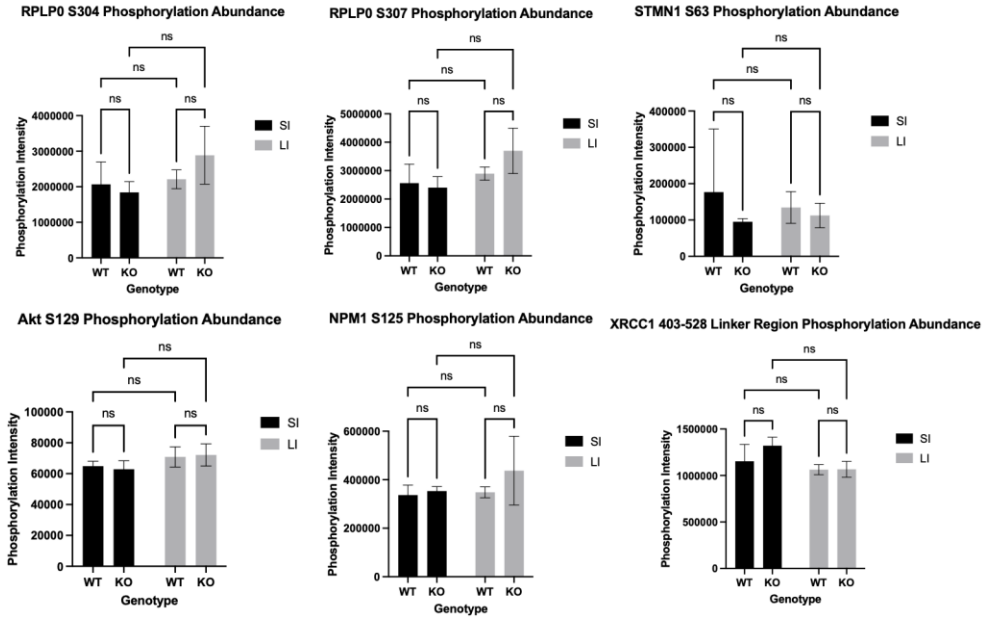

B.

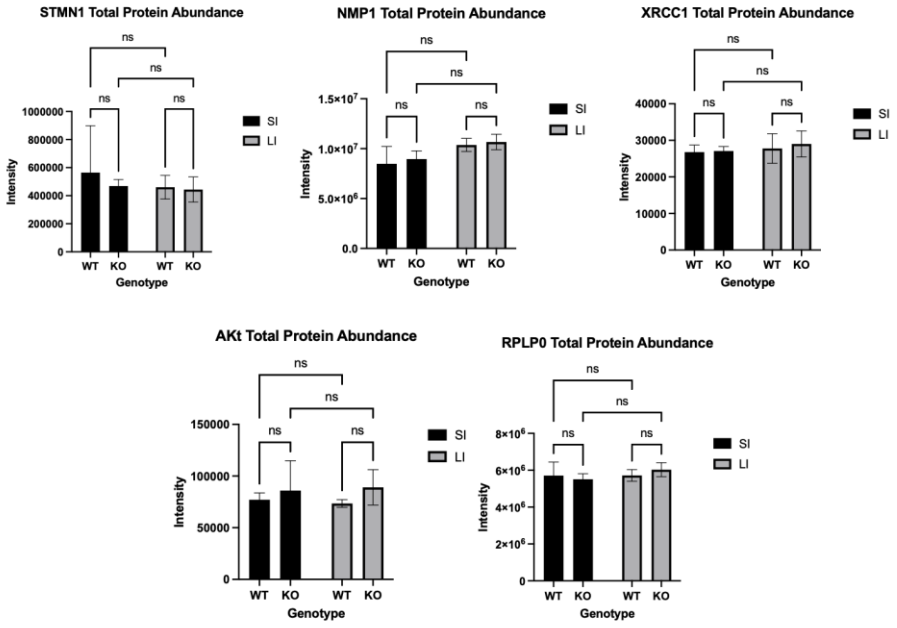

Figure 10: Bar Graphs of the abundance of Ck2 targets.
Image A shows the abundance of functionally important phosphorylated peptides. Image B shows their total protein abundance. Statistical comparisons done as mentioned above.

Ck2 phosphorylates the ribosomal P-stalk protein ul10 (RPLP0) at S304 and S307. This modification is imperative for ribosome biogenesis, ribosome function, and translation (Filipek et al., 2020). DNA repair protein XRCC1 was phosphorylated in its linker region, at multiple serine and threonine residues. This allows XRCC1 to facilitate DNA strand break repair and increases single-strand break repair after oxidative DNA damage (Strom et al., 2011). Stathmin 1 (STMN1) is a protein that is responsible for microtubule dynamics and was phosphorylated at S63. S63 phosphorylation is responsible for regular for microtubule stabilization and spindle formation (Liu et al., 2012). Nucleophosmin (NPM1) phosphorylation at S125 induces nucleolar organization and enhances nucleophosmin functions of transcription modulation, histone chaperoning, ribosome biogenesis, DNA repair, etc. (Sekhar et al., 2023). Lastly, the Akt kinase is phosphorylated at S129, which in turn phosphorylates Beta-catenin. B-catenin is a protein involved in cellular homeostasis, cell-cell adhesion, etc. This pathway was shown to increase survivin expression, preventing apoptosis (Ponce et al., 2010). The phospho-abundance of these peptides and total protein abundance were constant across genotypes and intestinal segments. Thus, it is unclear how, or if, Ck2 affected the phosphoproteome of our samples. A notable study found that Ck2 is required for IL-6-induced activation of STAT1/3 via JAK1. Inhibition of Ck2 inhibited STAT phosphorylation and in turn, inhibited cellular proliferation and inflammation (Aparacio-Siegmund et al., 2014). Our lab and others have shown this pathway is regulated in a similar manner by *Ptpn2* (Pan et al., 2022). It is interesting how both Ck2 and *Ptpn2* regulate this pathway, but it is unclear how they affect the pathway in the absence of each other. Evidently, p-STAT1

and p-STAT3 were still elevated in KO samples (Figure 5). There are no studies that evaluate the correlation of these Ck2 targets and *Ptpn2* in the intestinal epithelium. In addition, Ck2 abundance was not observed to be affected by the KO of *Ptpn2*. It was interesting to find out that occludin S408 phosphorylation (Figure 7, Image A) is catalyzed by Ck2 (Raleigh et al., 2011). This may be a reason why "actin cytoskeleton signaling" was an upregulated pathway. Knowing that lack of *Ptpn2* causes impairment of tight junctions, it was surprising to see p-S408 unchanged in KO samples, although it is important to point out that S408 cannot be a direct substrate of TCPTP given its exclusive role as a tyrosine phosphatase. Given the constant abundance of the Ck2 substrates, it is unlikely that these proteins are affected by loss of *Ptpn2*.

Kinome Analysis in *Ptpn2*-knockdown human intestinal epithelial cell lines

We performed an additional broad screening assay to determine more global effects of reduced *Ptpn2* activity in intestinal epithelial cells. Using *Ptpn2*-shRNA knockdown (KD) HT-29 (colorectal adenocarcinoma epithelial cells) cells, and control cells, we conducted kinome (subset of all kinases in a sample) analysis in collaboration with Dr. Yinsheng Wang's lab at UCR. Dr. Wang's lab performed Mass Spec. analysis of unchallenged and IFN-γ challenged control-shRNA vs. *Ptpn2*-KD HT-29 cells.

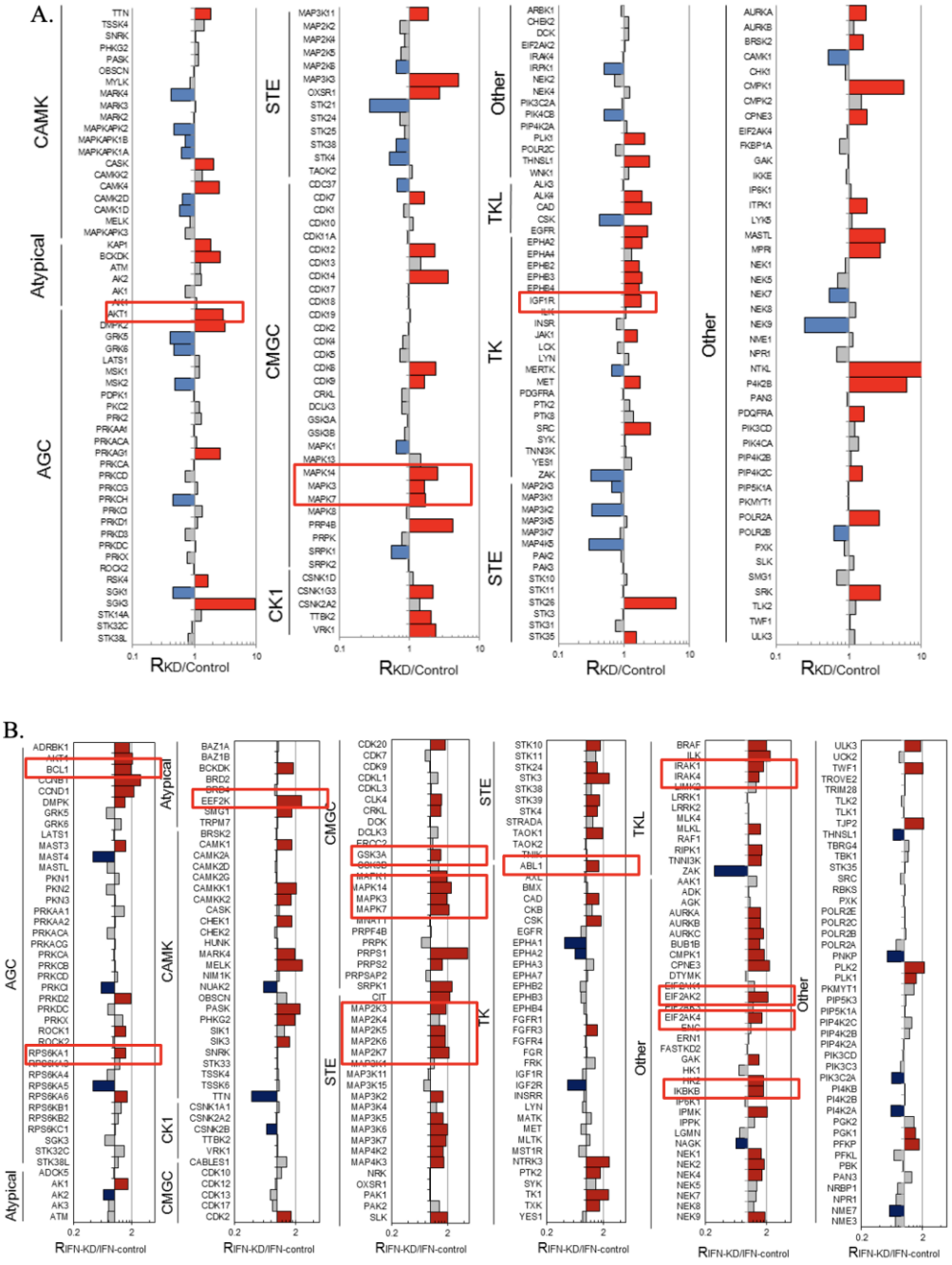

Figure 11: Kinome expression in HT-29 Cells:
Image A shows the kinase expression ratios in unchallenged shRNA-*Ptpn2* KD cells: control cells (Rkd/control). Image B shows kinase expression ratios in IFN-γ challenged cells between the same genotypes. Graphs were made from raw proteomic data. Upregulated kinases of interest in red rectangles.

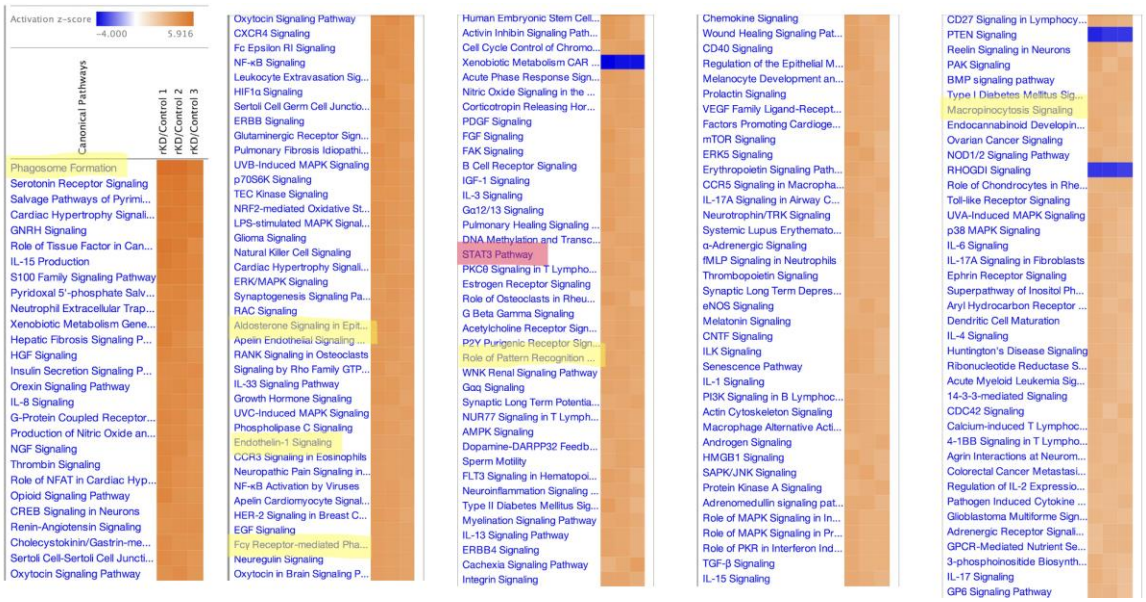

Figure 12: IPA pathway analysis of three samples representing the ratio of KD/WT cells.
Ratios of KD/WT kinase expression extracted from Mass Spec. analysis were entered into IPA for pathway analysis. Highlighted pathways are pathways that were also identified in the phosphoproteomic analysis, excluding STAT3 signaling.

Many of the upregulated kinases in Figure 11 are involved in cytokine signaling, cellular proliferation, cellular adhesion, etc. Figure 12 shows a robust and consistent representation of upregulated and downregulated pathways when *Ptpn2* is knocked down. Many of the upregulated pathways were cytokine signaling pathways, which is what we would expect to see since loss of *Ptpn2* upregulates the JAK-STAT pathway. There were also many upregulated disease pathways. This is also expected since loss of *Ptpn2* has been shown to lead to the onset of many diseases. Comparing figure 11 to figure 12, there is a direct correlation between the kinases and the pathways that were identified. A family of upregulated MAPK kinases indicated in Figure 11 correlate to the multiple "Role of MAPK signaling" and "p38 MAPK signaling" pathways in Figure 12. The Insulin Growth Factor 1 (IGF1R) kinase (Figure 11) is involved in IGF-1 signaling

(Figure 12). AKT1 is a mediator in Nf-kb signaling. IRAK1 (Image B, Figure 11) is associated with mTOR signaling, IRAK4 participates in toll-like receptor (TLR) pathways induced by LPS, IKBB also participates in Nf-kb signaling, and BCL-1 is involved in cell cycle control. In response to ER stress, EIF2AK2 serve as regulators in MAPK, IFN, and Nf-kb pathways and EIF2AK4 induces cell cycle arrest. ABL1 is a mediator of autophagy and cell survival. These are all pathways upregulated as shown in Figure 12. This is just to name a few. We expected to see patterns like these in our phosphoproteomic analysis. The most important observation is that some of the upregulated pathways in KO samples from the phosphoproteomic analysis were identified here as well. These include phagosome formation, aldosterone signaling in epithelial cells, actin cytoskeleton signaling, endothelin-1 signaling, Fcγ receptor-mediated phagocytosis, role of pattern recognition receptors, and macropinocytosis. The upregulation of these pathways is expected when there is excess inflammation, destabilization of tight junctions, and in general, disruption of the homeostasis of the intestinal epithelium caused by the loss of TCPTP.

DISCUSSION

Our major overall finding was that phosphoproteomic analysis is far from precise and failed to detect well-validated examples of tyrosine phosphorylated substrates that were separately probed as positive controls. We were unable to observe any major differences in the phosphoproteomic datasets between WT and KO samples, and there could be many reasons for that. The western blots in Figure 5 clearly showed the absence of TCPTP in KO samples and presence of the expected p-tyrosine residues of STAT1 and STAT3. This confirms that it was very unlikely a tissue sample preparation issue or lack of an effect of *Ptpn2* deletion. This may indicate that phosphoproteomic analysis via Mass Spec. lacks the sensitivity to capture phosphorylation differences in primary mouse isolated cells. Studies have shown that just using trypsin for protein digestion is not the most effective in identifying the highest amount of peptides. It is recommended to use other proteases accompanied with trypsin to achieve the best peptide coverage (Gilmore et al., 2012). This may have particularly impinged upon detection of phosphorylated tyrosine residues, specifically the critical STAT1 and STAT3 tyrosine residues, which are less abundant than Ser/Thr residues (Brady & Lau, 2012).

The IPA software was also not as informative as had been hoped. This was likely hampered by the lack of sensitivity in the mass spec data but may also reflect a lack of optimization for phosphoproteomic datasets currently. IPA did not show the specific phosphorylated proteins that caused the upregulation of pathways, nor did it show which pathways were correlated with the top upstream kinases. It only showed a list of the top substrates of a particular kinase, but no further analysis. In addition, IPA did not show

how the phosphorylation of a specific residue affected the function of a protein. All of this, combined with the inconsistent z-scores between WT and KO samples, made it impossible to make distinctions between WT and KO. Even though IPA interpreted Csn2ka1 (Ck2) to be downregulated in both genotypes, the total protein data clearly showed it was not. While the use of other proteomic analysis software programs for pathway and upstream kinase analysis may identify some additional pathways of interest, this approach will still be severely constrained by the lack of detectable differences in the mass spec. datasets.

An additional consideration is that even though our isolated intestinal samples were predominantly comprised of IECs, there was still some contamination from fibroblasts and other mesenchymal cells as indicated by western blotting. While the presence of these cells may have skewed the results possibly through dilution or these cells exhibiting opposing phosphorylation patterns compared to IECs, this was not an issue in the detection of bona fide *Ptpn2* substrates (STAT1 and STAT3) that exhibited increased tyrosine phosphorylation via western blot. Thus, it is highly unlikely that the presence of non-epithelial cells contributed to the lack of sensitivity of the phosphoproteomic analysis.

The kinome analysis (Figures 11&12) identified that some pathways found to be upregulated by this technique were also upregulated in the phosphoproteomic analysis. This suggests that our phosphoproteomic analysis of mouse IECs wasn't entirely without success. The kinome data reflects the ratio of unchallenged and IFN-γ challenged *Ptpn2*-KD to control-shRNA cells and displays much greater consistency than the mouse data.

Of course, the kinome data samples were obtained solely from a homogeneous epithelial cell line (HT-29), unlike the samples from mice which comprised heterogeneous epithelial phenotypes (absorptive vs. secretory lineages) and mesenchymal cells. In the future, it will be interesting to test if phosphoproteomic analysis may prove to be more sensitive in essentially isogenic cell lines than mixed primary cell populations isolated from native tissue.

In conclusion, this study identified important limitations with a broad 'omic' screening approach that failed to detect established phosphorylated targets known to be upregulated by reduced activity or expression of *Ptpn2* across multiple model systems. The lack of sensitivity of the mass spec. may have been caused by a nonoptimal tryptic digestion-based assay. An additional factor may be a lack of sensitivity in detecting differential phosphorylation of tyrosine residues which are less abundant that serine and threonine residues. Inconsistent pathway and upstream kinase data may have resulted from the use of mixed primary isolated intestinal epithelial cells versus the more homogenous cell line samples used for kinome analysis. While the overall findings of the phosphoproteomic analysis were less than satisfactory, we were able to salvage this study by including kinome analysis of *Ptpn2*-KD cells which revealed specific kinases and associated pathways that will provide ample avenues for further investigation. These future studies will help to further increase our understanding of mechanisms by which loss of *Ptpn2* activity modifies cellular pathways involved in established *Ptpn2*-regulated functions (proliferation, barrier function, immune cell regulation, etc.), as well as identify

additional roles for *Ptpn2* in the regulation of epithelial homeostasis and inflammatory responses.

BIBLIOGRAPHY

Altay, G., Batlle, E., Fernández-Majada, V., & Martinez, E. (2020). In vitro Self-organized Mouse Small Intestinal Epithelial Monolayer Protocol. *Bio-Protocol*, *10*(3), e3514. https://doi.org/10.21769/BioProtoc.3514

Aparicio-Siegmund, S., Sommer, J., Monhasery, N., Schwanbeck, R., Keil, E., Finkenstädt, D., Pfeffer, K., Rose-John, S., Scheller, J., & Garbers, C. (2014). Inhibition of protein kinase II (CK2) prevents induced signal transducer and activator of transcription (STAT) 1/3 and constitutive STAT3 activation. *Oncotarget*, *5*(8), 2131–2148. https://doi.org/10.18632/oncotarget.1852

Borgo, C., D'Amore, C., Sarno, S., Salvi, M., & Ruzzene, M. (2021). Protein kinase CK2: a potential therapeutic target for diverse human diseases. *Signal Transduction and Targeted Therapy*, *6*(1), 183. https://doi.org/10.1038/s41392-021-00567-7

Brady, S. T., & Lau, L.-F. (2012). Tyrosine Phosphorylation. In *Basic Neurochemistry* (pp. 493–513). Elsevier. https://doi.org/10.1016/B978-0-12-374947-5.00026-2

Buchowiecka, A. K. (2014). Puzzling over protein cysteine phosphorylation – assessment of proteomic tools for S-phosphorylation profiling. *The Analyst*, *139*(17), 4118–4123. https://doi.org/10.1039/C4AN00724G

Canale, V., Spalinger, M. R., Alvarez, R., Sayoc-Becerra, A., Sanati, G., Manz, S., Chatterjee, P., Santos, A. N., Lei, H., Jahng, S., Chu, T., Shawki, A., Hanson, E., Eckmann, L., Ouellette, A. J., & McCole, D. F. (2023). PTPN2 Is a Critical Regulator of Ileal Paneth Cell Viability and Function in Mice. *Cellular and Molecular Gastroenterology and Hepatology*, *16*(1), 39–62. https://doi.org/10.1016/j.jcmgh.2023.03.009

Díaz-Coránguez, M., Liu, X., & Antonetti, D. A. (2019). Tight Junctions in Cell Proliferation. *International Journal of Molecular Sciences*, *20*(23), 5972. https://doi.org/10.3390/ijms20235972

Elias, B. C., Suzuki, T., Seth, A., Giorgianni, F., Kale, G., Shen, L., Turner, J. R., Naren, A., Desiderio, D. M., & Rao, R. (2009). Phosphorylation of Tyr-398 and Tyr-402 in Occludin Prevents Its Interaction with ZO-1 and Destabilizes Its Assembly at the Tight Junctions. *Journal of Biological Chemistry*, *284*(3), 1559–1569. https://doi.org/10.1074/jbc.M804783200

Filipek, K., Michalec-Wawiórka, B., Boguszewska, A., Kmiecik, S., & Tchórzewski, M. (2020). Phosphorylation of the N-terminal domain of ribosomal P-stalk protein uL10 governs its association with the ribosome. *FEBS Letters*, *594*(18), 3002–3019. https://doi.org/10.1002/1873-3468.13885

Fuhrmann, J., Clancy, K. W., & Thompson, P. R. (2015). Chemical Biology of Protein Arginine Modifications in Epigenetic Regulation. *Chemical Reviews*, *115*(11), 5413–5461. https://doi.org/10.1021/acs.chemrev.5b00003

Gilmore, J. M., Kettenbach, A. N., & Gerber, S. A. (2012). Increasing phosphoproteomic coverage through sequential digestion by complementary proteases. *Analytical and Bioanalytical Chemistry*, *402*(2), 711–720. https://doi.org/10.1007/s00216-011-5466-5

Hardman, G., Perkins, S., Brownridge, P. J., Clarke, C. J., Byrne, D. P., Campbell, A. E., Kalyuzhnyy, A., Myall, A., Eyers, P. A., Jones, A. R., & Eyers, C. E. (2019). Strong anion exchange-mediated phosphoproteomics reveals extensive human non-canonical phosphorylation. *The EMBO Journal*, *38*(21), e100847. https://doi.org/10.15252/embj.2018100847

Kassambara, Alboukadel. 2023. Ggpubr: 'Ggplot2' Based Publication Ready Plots. https://CRAN.R-project.org/package=ggpubr.

Kim, M., Morales, L. D., Jang, I.-S., Cho, Y.-Y., & Kim, D. J. (2018). Protein Tyrosine Phosphatases as Potential Regulators of STAT3 Signaling. *International Journal of Molecular Sciences*, *19*(9). https://doi.org/10.3390/ijms19092708

Kovarik, P., Stoiber, D., Eyers, P. A., Menghini, R., Neininger, A., Gaestel, M., Cohen, P., & Decker, T. (1999). Stress-induced phosphorylation of STAT1 at Ser727 requires p38 mitogen-activated protein kinase whereas IFN-gamma uses a different signaling pathway. *Proceedings of the National Academy of Sciences of the United States of America*, *96*(24), 13956–13961. https://doi.org/10.1073/pnas.96.24.13956

Krämer, A., Green, J., Pollard, J., Jr, & Tugendreich, S. (2014). Causal analysis approaches in Ingenuity Pathway Analysis. *Bioinformatics (Oxford, England)*, *30*(4), 523–530. https://doi.org/10.1093/bioinformatics/btt703

Krishnan, M., & McCole, D. F. (2017). T cell protein tyrosine phosphatase prevents STAT1 induction of claudin-2 expression in intestinal epithelial cells. *Annals of the New York Academy of Sciences*, *1405*(1), 116–130. https://doi.org/10.1111/nyas.13439

Lapek, J. D., Tombline, G., Kellersberger, K. A., Friedman, M. R., & Friedman, A. E. (2015). Evidence of histidine and aspartic acid phosphorylation in human prostate cancer cells. *Naunyn-Schmiedeberg's Archives of Pharmacology*, *388*(2), 161–173. https://doi.org/10.1007/s00210-014-1063-4

Lin, W.-H., Chang, Y.-W., Hong, M.-X., Hsu, T.-C., Lee, K.-C., Lin, C., & Lee, J.-L. (2021). STAT3 phosphorylation at Ser727 and Tyr705 differentially regulates the EMT-

MET switch and cancer metastasis. *Oncogene*, *40*(4), 791–805. https://doi.org/10.1038/s41388-020-01566-8

LIU, F., SUN, Y.-L., XU, Y., LIU, F., WANG, L.-S., & ZHAO, X.-H. (2013). Expression and phosphorylation of stathmin correlate with cell migration in esophageal squamous cell carcinoma. *Oncology Reports*, *29*(2), 419–424. https://doi.org/10.3892/or.2012.2157

Marchelletta, R. R., Krishnan, M., Spalinger, M. R., Placone, T. W., Alvarez, R., Sayoc-Becerra, A., Canale, V., Shawki, A., Park, Y. S., Bernts, L. H., Myers, S., Tremblay, M. L., Barrett, K. E., Krystofiak, E., Kachar, B., McGovern, D. P., Weber, C. R., Hanson, E. M., Eckmann, L., & McCole, D. F. (2021). T cell protein tyrosine phosphatase protects intestinal barrier function by restricting epithelial tight junction remodeling. *The Journal of Clinical Investigation*, *131*(17). https://doi.org/10.1172/JCI138230

Mazurkiewicz-Munoz, A. M., Argetsinger, L. S., Kouadio, J.-L. K., Stensballe, A., Jensen, O. N., Cline, J. M., & Carter-Su, C. (2006). Phosphorylation of JAK2 at serine 523: a negative regulator of JAK2 that is stimulated by growth hormone and epidermal growth factor. *Molecular and Cellular Biology*, *26*(11), 4052–4062. https://doi.org/10.1128/MCB.01591-05

McCole, D. F. (2013). Phosphatase regulation of intercellular junctions. *Tissue Barriers*, *1*(5), e26713. https://doi.org/10.4161/tisb.26713

Nitulescu, I. I., Meyer, S. C., Wen, Q. J., Crispino, J. D., Lemieux, M. E., Levine, R. L., Pelish, H. E., & Shair, M. D. (2017). Mediator Kinase Phosphorylation of STAT1 S727 Promotes Growth of Neoplasms With JAK-STAT Activation. *EBioMedicine*, *26*, 112–125. https://doi.org/10.1016/j.ebiom.2017.11.013

Núñez de Villavicencio-Díaz, T., Mazola, Y., Perera Negrín, Y., Cruz García, Y., Guirola Cruz, O., & Perea Rodríguez, S. E. (2015). Predicting CK2 beta-dependent substrates using linear patterns. *Biochemistry and biophysics reports*, *4*, 20–27. https://doi.org/10.1016/j.bbrep.2015.08.011

Ostrowska-Podhorodecka, Z., Ding, I., Norouzi, M., & McCulloch, C. A. (2022). Impact of Vimentin on Regulation of Cell Signaling and Matrix Remodeling. *Frontiers in Cell and Developmental Biology*, *10*. https://doi.org/10.3389/fcell.2022.869069

Pan, J., Zhou, L., Zhang, C., Xu, Q., & Sun, Y. (2022). Targeting protein phosphatases for the treatment of inflammation-related diseases: From signaling to therapy. *Signal Transduction and Targeted Therapy*, *7*(1), 177. https://doi.org/10.1038/s41392-022-01038-3

Ponce, D. P., Maturana, J. L., Cabello, P., Yefi, R., Niechi, I., Silva, E., Armisen, R., Galindo, M., Antonelli, M., & Tapia, J. C. (2011). Phosphorylation of AKT/PKB by CK2 is necessary for the AKT-dependent up-regulation of β-catenin transcriptional activity. *Journal of Cellular Physiology*, *226*(7), 1953–1959. https://doi.org/10.1002/jcp.22527

R Core Team. 2022. R: A Language and Environment for Statistical Computing. Vienna, Austria: R Foundation for Statistical Computing. https://www.R-project.org/.

Raleigh, D. R., Boe, D. M., Yu, D., Weber, C. R., Marchiando, A. M., Bradford, E. M., Wang, Y., Wu, L., Schneeberger, E. E., Shen, L., & Turner, J. R. (2011). Occludin S408 phosphorylation regulates tight junction protein interactions and barrier function. *The Journal of Cell Biology*, *193*(3), 565–582. https://doi.org/10.1083/jcb.201010065

Rosales, M., Pérez, G. V, Ramón, A. C., Cruz, Y., Rodríguez-Ulloa, A., Besada, V., Ramos, Y., Vázquez-Blomquist, D., Caballero, E., Aguilar, D., González, L. J., Zettl, K., Wiśniewski, J. R., Yang, K., Perera, Y., & Perea, S. E. (2021). Targeting of Protein Kinase CK2 in Acute Myeloid Leukemia Cells Using the Clinical-Grade Synthetic-Peptide CIGB-300. *Biomedicines*, *9*(7), 766. https://doi.org/10.3390/biomedicines9070766

Savage, R. S., & Zhang Bing. (2020). Using phosphoproteomics data to understand cellular signaling: a comprehensive guide to bioinformatics resources. *Clinical Proteomics*, *17*(27).

Sayoc-Becerra, A., Krishnan, M., Fan, S., Jimenez, J., Hernandez, R., Gibson, K., Preciado, R., Butt, G., & McCole, D. F. (2019). The JAK-Inhibitor Tofacitinib Rescues Human Intestinal Epithelial Cells and Colonoids from Cytokine-Induced Barrier Dysfunction. *Inflammatory Bowel Diseases*, *26*(3), 407–422. https://doi.org/10.1093/ibd/izz266

Sekhar, K. R., & Freeman, M. L. (2023). Nucleophosmin Plays a Role in Repairing DNA Damage and Is a Target for Cancer Treatment. *Cancer Research*, *83*(10), 1573–1580. https://doi.org/10.1158/0008-5472.CAN-22-3631

Shigetomi, K., & Ikenouchi, J. (2018). Regulation of the epithelial barrier by post-translational modifications of tight junction membrane proteins. *The Journal of Biochemistry*, *163*(4), 265–272. https://doi.org/10.1093/jb/mvx077

Spalinger, M. R., Manzini, R., Hering, L., Riggs, J. B., Gottier, C., Lang, S., Atrott, K., Fettelschoss, A., Olomski, F., Kündig, T. M., Fried, M., McCole, D. F., Rogler, G., & Scharl, M. (2018). PTPN2 Regulates Inflammasome Activation and Controls Onset of Intestinal Inflammation and Colon Cancer. *Cell Reports*, *22*(7), 1835–1848. https://doi.org/10.1016/j.celrep.2018.01.052

Spalinger, M. R., Sayoc-Becerra, A., Santos, A. N., Shawki, A., Canale, V., Krishnan, M., Niechcial, A., Obialo, N., Scharl, M., Li, J., Nair, M. G., & McCole, D. F. (2020). PTPN2 Regulates Interactions Between Macrophages and Intestinal Epithelial Cells to Promote Intestinal Barrier Function. *Gastroenterology*, *159*(5), 1763-1777.e14. https://doi.org/10.1053/j.gastro.2020.07.004

Ström, C. E., Mortusewicz, O., Finch, D., Parsons, J. L., Lagerqvist, A., Johansson, F., Schultz, N., Erixon, K., Dianov, G. L., & Helleday, T. (2011). CK2 phosphorylation of XRCC1 facilitates dissociation from DNA and single-strand break formation during base excision repair. *DNA Repair*, *10*(9), 961–969. https://doi.org/10.1016/j.dnarep.2011.07.004

Van Itallie, C. M., & Anderson, J. M. (2018). Phosphorylation of tight junction transmembrane proteins: Many sites, much to do. *Tissue Barriers*, *6*(1), e1382671. https://doi.org/10.1080/21688370.2017.1382671

Wickham, Hadley, Mara Averick, Jennifer Bryan, Winston Chang, Lucy McGowan, Romain François, Garrett Grolemund, et al. 2019. "Welcome to the Tidyverse." J. Open Source Softw. 4 (43): 1686.